Excited State Proton Transfer Dynamics of Topotecan Inside Biomimicking Nanocavity

ARTICLE *in* THE JOURNAL OF PHYSICAL CHEMISTRY B · AUGUST 2014

Impact Factor: 3.3 · DOI: 10.1021/jp5066902 · Source: PubMed

THE JOURNAL OF PHYSICAL CHEMISTRY B

Article

pubs.acs.org/JPCB

Excited State Proton Transfer Dynamics of Topotecan Inside Biomimicking Nanocavity

Raj Kumar Koninti, Krishna Gavvala, Abhigyan Sengupta, and Partha Hazra*

Department of Chemistry, Indian Institute of Science Education and Research (IISER), Pune 411008, Maharashtra, India

Supporting Information

ABSTRACT: The excited state proton transfer (ESPT) dynamics of a potentially important anticancer drug, Topotecan (TPT), has been explored in aqueous reverse micelle (RM) using steady-state and time-resolved fluorescence measurements. Both the time-resolved emission spectrum and time-resolved area normalized emission spectrum infer the generation of excited state zwitterionic form of TPT from the excited state cationic form of TPT, as a result of ESPT process from the −OH group of TPT to the nearby water molecule. The ESPT dynamics were found to be severely retarded inside the nanocavities of RMs, yielding time constants of 250 ps to 1.0 ns, which is significantly slower than the dynamics obtained in bulk water (32 ps). The observed slow ESPT dynamics in RM compared to bulk water is mainly attributed to the sluggish hydrogen-bonded network dynamics of water molecules inside the nanocavity of RM and the screening of the sodium ions present at the interface.

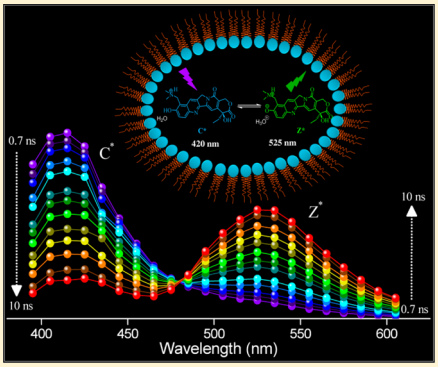

1. INTRODUCTION

Topotecan (TPT) is a water-soluble analogue of camptothecin (CPT), a pentacyclic alkaloid belonging to a class of antitumoral agents.[1−4] TPT is found to be a potential inhibitor for the growth of tumor cell through a unique mechanism by which it reduces the activity of the human topoisomerase I (Top1) enzyme through the formation of a Top1−DNA complex;[2,3,5−8] thereby, stabilizing the cleavable Top1−DNA complex that collides with the progression of the replication fork, producing lethal double strand DNA break and cell death.[4,9,10] TPT consists of five rings, of which four (A, B, D, and E) are six-membered and one (C) is five-membered. The H atoms on the 9- and 10-positions of the A-ring in CPT are replaced by dimethylaminomethylene and hydroxyl groups, respectively.[11−14] These extra functional groups on TPT enhance the solubility in physiological medium and reduce the cytotoxicity to human tissues.[4,6−8] Hence, TPT has been a clinically approved anticancer drug for the treatment of several cancers.[4,6−8] The presence of 6-hydroxyquinoline (6HQ, A- and B-rings) subunit and the 9-dimethylaminomethylene group leads to the existence of different protolytic forms of TPT in the ground as well as excited states. Nunzio et al. reported elaborative pH-dependent studies and solvent effect on the structural aspects of TPT, and it was found that TPT exists in different protolytic forms, such as enol (E), cationic (C), and zwitterionic (Z) forms, depending on the pH as well as the solvent.[13,14] Although in ground state, the drug exists in different forms (E, C, and Z), and interestingly, TPT exhibits a single fluorescence peak (∼530 nm) in aqueous solution (at physiological pH) responsible for the emission from Z*, which is believed to be an outcome from the excited-state proton transfer (ESPT) from −OH group of TPT to water.[13−16] It was also found that the ESPT process in TPT is sensitive to polarity,[14] and thus, the excited-state photophysics of TPT can be modulated inside the nanocavities of a supramolecular host, such as cyclodextrin, calixarene, cucurbituril, and so forth. In continuation of this effort, Gavvala et al. reported that the ESPT process of TPT is inhibited inside the cucurbit[7]uril (CB7) nanocavity.[15] Although it has been shown that the stability as well as photophysics of the drug can be modulated by encapsulating the drug into liposomes,[17] cyclodextrins,[16,18] calixarene,[19] and cucurbituril,[15] no focus has been made on modulating the ESPT process of TPT inside biological nanocavities, where water was often confined in a small pocket of a membrane.

The reverse micelle (RM) is a nanometer-sized water droplet surrounded by a layer of surfactant molecules immersed in a nonpolar solvent. The unique confinement effect of RMs has been used as a model system of various biological environments, such as, protein pockets and cell membranes.[20−25] RMs have also been extensively used in enzymatic reactions and chemical catalysis.[26,27] The size of the confined "water pool" depends on the w_0 value, where w_0 = [water]/[AOT].[25,28] As the w_0 increases, the solvent pool diameter usually increases with simultaneous changes in the local environment within the pools. For water RMs, the radius (r_{max}) of water droplet is 2.3w_0 Å.[28,29] The studies of the water confined inside the RM suggest that water at the interface is largely different from those of the

Special Issue: Photoinduced Proton Transfer in Chemistry and Biology Symposium

Received: July 4, 2014
Revised: August 7, 2014
Published: August 8, 2014

dx.doi.org/10.1021/jp5066902 | J. Phys. Chem. B 2015, 119, 2363−2371

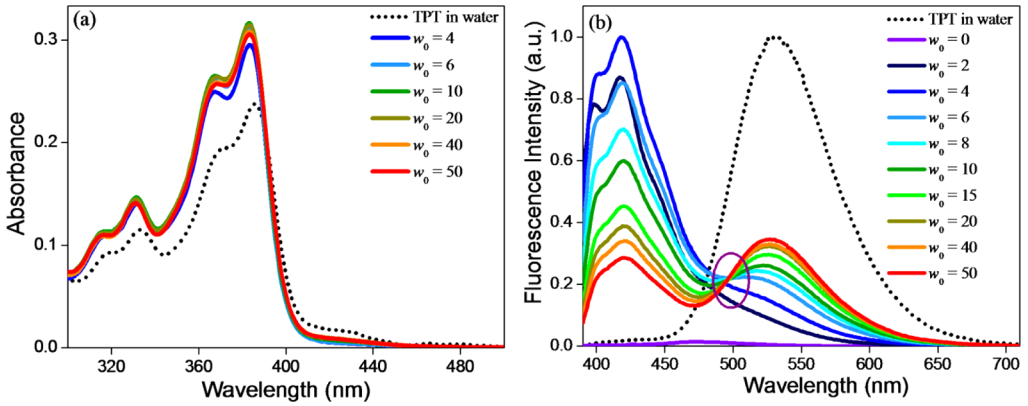

Figure 1. (a) Absorption spectra and (b) steady-state emission profiles of TPT in water (·····) and in AOT reverse micelles with progressively increasing water content (w_0).

bulk, while the water at the "central pool" approaches to the properties of bulk water.[20,22−25,28,30−40] The confinement effect of nanopools and enclosing interfacial surfaces modulate physical properties of water, such as the H-bonding ability and polarity, which are the primary elements for the proton transfer process in water. Numerous spectroscopic studies infer that inhomogeneous dynamics of water inside the RM is attributed to the differential H-bonding behavior in two different regions of RMs.[30,34,36−38,40−53] Recently, proton transfer attracts burgeoning interest to the researchers due to its key role in a variety of biological and chemical processes.[54,55] In continuation of this effort, fluorescence probes sensitive to H bonding and proton transfer reactions are often probed in the reverse micellar environments due to the above-mentioned unique features.[29,39,49−51,56−65] Herein, we report the encapsulation of TPT inside aqueous RMs and the consequences of confinement on photophysical properties of TPT using steady-state and time-resolved spectroscopic techniques. The prime focus of this work is to understand the effect of nanoconfinement and polarity on excited-state proton transfer (ESPT) dynamics of TPT. Interestingly, we have observed that ESPT dynamics is dramatically slowed down when the drug molecules are encapsulated inside the RMs and result in emission mainly from zwitterionic forms of TPT. The time-resolved emission spectrum (TRES) and time-resolved area normalized emission spectrum (TRANES) provide information about the existence of multiple emissive species in the excited state. We believe that our results might provide a new insight toward the understanding of fluorescence properties of TPT inside a cellular-like environment, and therefore, delivery of TPT inside the cell can easily be monitored by advanced imaging techniques.

2. EXPERIMENTAL SECTION

Topotecan (high purity, ≥99%), sodium bis(2-ethyl-1-hexyl) sulfosuccinate (AOT) (Ultra >99.0%), and deuterium oxide (high purity, 99.9%) were purchased from Sigma-Aldrich and used without further purification. *n*-Heptane of spectroscopy grade was obtained from Spectrochem Pvt. Ltd. India and used as received. AOT was properly dried under vacuum pump about 48 h before preparing RM. TPT was directly added to *n*-heptane solvent and sonicated for 15 min for uniform distribution of drug molecules. After that, AOT (0.1 M) was added to the above-mentioned solution, and a clear transparent solution was observed. The concentration of AOT was kept at 0.1 M for all measurements. RM of various w_0 values were prepared by the addition of an appropriate amount of Milli-Q water to the AOT/*n*-heptane system. Steady-state absorption and emission measurements were performed on a Shimadzu UV−visible spectrophotometer (UV-2600, Japan) and a Fluoromax-4 spectrofluorimeter (Horiba Jobin Yvon), respectively. Fluorescence decays were collected by time-correlated single photon counting (TCSPC) setup from Horiba Jobin Yvon. The detailed description of the instrument appears elsewhere.[66,67] Briefly, we have used 375 nm diode Laser (IBH, UK, NanoLED-375L) having a fwhm of <100 ps as an excitation source both for lifetime as well as anisotropy studies. The fluorescence signals were collected at a magic angle using a MCP-PMT (Hamamatsu, Japan) detector. Time-resolved emission spectra (TRES) were constructed from the decays measured at different wavelengths of emission with a spectral interval typically of 10 nm. Time-resolved area normalized emission spectra (TRANES) have been constructed by area normalization of these TRES. The time-resolved fluorescence anisotropy decay function, $r(t)$, was calculated from using the following equation:

$$r(t) = \frac{I_{\parallel}(t) - GI_{\perp}(t)}{I_{\parallel}(t) + 2GI_{\perp}(t)}$$

where G is the correction factor for detector sensitivity to the polarization direction of the emission. $I_{\parallel}(t)$ and $I_{\perp}(t)$ are the time-dependent intensities of the fluorescence decays polarized parallel and perpendicular, respectively, to the polarization of the excitation light. For time-resolved anisotropy studies, we have used a motorized polarizer in the emission side. The emission intensities at perpendicular and parallel polarizations were collected alternatively for 60 s. For typical anisotropy decay, the difference between the peak counts at parallel and perpendicular polarization was kept to 10000. The G factor of the setup was measured using variable orientation of the polarizer. The excitation polarizer remained fixed at the horizontal position. The emission polarizer repetitively changed its position from vertical [resulting decay $I_{\perp}(t)$] to horizontal [resulting decay $I_{\parallel}(t)$] with a 60 s time duration for each. The analysis of lifetime and anisotropy data was done by IBH DAS6 analysis software. We have fitted both lifetime as well as anisotropy data with a minimum number of exponentials. The quality of fitting was judged by the χ^2 value, and the value close to 1 was considered as a good fit.

dx.doi.org/10.1021/jp5066902 | J. Phys. Chem. B 2015, 119, 2363−2371

3. RESULTS AND DISCUSSION

3.1. Steady-State Measurements. The UV−visible absorption spectra of TPT with increasing water content of the RM are depicted in Figure 1a. Absorption spectra of TPT in water-RM exhibit three characteristic bands in the region of 250−410 nm, irrespective of the water content of RM. The absorption maximum at ∼380 nm along with a shoulder at 368 nm is mainly attributed to the $\pi-\pi^*$ transition of quinoline moiety present in the TPT.[14] With increasing water content of the RM, although the band positions are not changing, the absorbance is enhanced. The solubility of TPT in *n*-heptane is low; however, in the presence of AOT and water, the solubility enhances significantly. The increased absorbance may be an outcome of increased solubility of TPT in the presence of AOT and water. Notably, a small shoulder at ∼410 nm, which is believed to appear from the zwitterionic form of TPT,[13−15] is observed at higher w_0 values of the water-RM.

Figure 1b depicts the steady-state emission profiles of TPT with increasing water content of the RM upon excitation at 380 nm. Emission of TPT in *n*-heptane is negligibly small, as the solubility of drug in *n*-heptane is very low. However, in the presence of AOT (w_0 = 0), a broad emission profile of TPT appears, indicating that the solubility of TPT takes place in the presence of the surfactant. With the introduction of water to the system (w_0 = 2), an intense peak at 420 nm is observed. On further addition of water (w_0 = 4), a shoulder at 515 nm is clearly visible along with a slight enhancement at a 420 nm peak. The addition of water (w_0 > 4) results in prominent appearance of a peak at ∼515 nm along with concomitant decrement in intensity of a higher energy peak. Upon further addition of water, the lower energy peak exhibits a red shift along with the hike in intensity, whereas the intensity of a high energy peak gradually decreases. As the emission property of TPT is highly dependent on the local hydrogen-bonding network,[13] the observed phenomena are attributed to the differential hydrogen-bonding network inside RM. It is already reported that 420 nm emission bands appears from the excited state cationic (C*) form (Scheme 1) of TPT.[13−16] Therefore, the initial increment in the emission intensity at 420 nm clearly suggests that reverse micellar environment facilitates the stabilization of cationic form of TPT (C-TPT). It is possible that C-TPT is involved in electrostatic interaction with the negatively charged polar head groups of AOT, and this interaction provides extra stabilization for cationic form of the drug inside the RM. As a result, cationic form is the dominant species inside RM at w_0 < 5 and is reflected in the emission profiles of TPT. It is well established that the zwitterionic (Z*) (Scheme 1) form of TPT emits around 520 nm.[13−16] Thus, the appearance of a peak at ∼515 nm after a certain w_0 value indicates the formation of the zwitterionic (Z*) form of TPT. Notably, although we are selectively exciting the C form (at 380 nm) of TPT, emission is detected from both zwitterionic as well as cationic forms. Therefore, Z* form is generated at the cost of C* as a result of the excited state intermolecular proton transfer (ESPT) process from the −OH group of TPT to the surrounding water molecule.

Scheme 1. Different Prototropic Forms of Topotecan

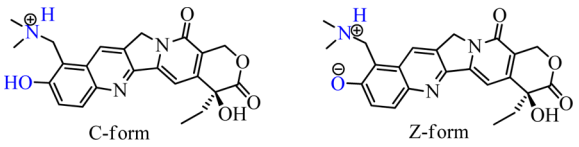

Water plays a pivotal role for the proton transfer reaction due to its H-bond accepting and conducting properties. Water is also recognized as an active participant in the transport mechanism of the proton as well as in the stabilization of an ion pair.[48] Initial addition of water to the AOT containing *n*-heptane solution causes all the water molecules to be trapped in the bound layers of the AOT surfactant. The physical properties of these interfacial "bound" water molecules are considerably different from the bulk water, as they are involved in strong H-bond interactions with the head groups of AOT and, thereby, shows higher viscosity, lower mobility, lower polarity, and a diminished intrasolvent H-bonding network.[20−25,28,31,40,68,69] Moreover, the pH of the water molecules associated with the sulfonate groups in the nanocavity is less than the bulk pH, as the hydronium ions of water are attracted toward the negatively charged sulfonate groups.[24,70] Under the condition where the number of available water molecules are reduced and/or where the structure of water is partially broken, the probability of proton transfer is reduced.[48] Thus, the conversion from C* to Z*, which is accompanied by the excited state proton abstraction from the −OH group of the TPT by the water molecule, is restricted inside RM. Notably, it was found that the extent of ESPT process is not efficient at lower w_0 values. For example, Spry et al. reported that the extent of ESPT of HPTS reduces significantly at a lower w_0 value of the RM.[56] Very recently, Sarkar and co-workers also found the intermolecular ESPT in water-RM begins at w_0 = 8 and increases with increasing w_0 value.[62] Therefore, our observations are consistent with the literature reports. The fact that the quenching efficiency of the C* emission grows monotonically and at the same time the emission of the Z* form increases (Figure 1b) with increasing w_0, suggests that the hydrogen bond plays an important role for the formation as well as stabilization of Z*-TPT. When the size of the RM is small, the coupled core−shell hydrogen bond network has hydrogen bond dynamics that are substantially slower than those of bulk water[30,52,53,56] and reduce the extent of excited-state proton transfer rate. As the w_0 value of the RM increases, the number of "bound" water molecules, which are engaged in the hydrogen-bonding interaction with SO^{3-} of AOT, decreases and at the same time the population of "free" water molecules is enhanced at the core of RM.[20−24,32] Therefore, it is expected that the extent of proton activity (H-bonding interactions) accelerates with increasing percentage of "free" water in RM, and thereby, facilitates the conversion of C* to Z*. The above observation is in good agreement with the literature report, where it was found that water molecules start forming a "water pool" inside the RM, at w_0 > 5.[29,35,59,62,71] The red shift in the emission peak of Z*-TPT indicates the migration of TPT molecules from the interfacial region toward the central region of the RM. Interestingly, unlike single emission from Z* form in bulk water, we have observed emission from both C* as well as Z* forms of TPT, even at the highest w_0 value of the RM. This suggests that some TPT molecules are still residing near the AOT group of the RM, where proton activity is not sufficient for the transformation of C* to Z*. Notably, the appearance of an iso-emissive point at ∼495 nm in the emission profiles suggests the existence of equilibrium between C and Z forms of TPT in the excited state. Interestingly, at the highest water content of the RM, the emission spectra does not match with

dx.doi.org/10.1021/jp5066902 | J. Phys. Chem. B 2015, 119, 2363−2371

that of the pure water spectrum, indicating the photopyrolytic reaction of the drug is being modulated inside the RM.

3.2. Fluorescence Lifetime Measurements. The time-resolved fluorescence decays of TPT in dry AOT and after addition of water were collected at the corresponding emission maxima of cationic and zwitterionic forms exciting at 375 nm. The fluorescence transients of C*-TPT in water-RMs at their corresponding emission maxima are depicted in Figure 2a, and the results are tabulated in Table 1. The decay profile of C*-TPT at any w_0 value consists of two lifetime components. For example, fluorescence transient at w_0 = 4 exhibits two lifetime components, 720 ps (22%) and 2 ns (78%). The biexponential nature of decay profile indicates that the drug molecules experience a heterogeneous environment inside the RM. With raising water content of the RM, percentage contribution of the short lifetime component (~700 ps) continuously enhances, whereas the percentage contribution of a long lifetime component (~2 ns) gradually reduces. Notably, increasing water content of the RM, the percentage of "free" water molecules responsible for the formation of "water pool" also increases.[20−24,28,71] The results indicate that the 2 ns component, whose contribution diminishes as w_0 value increases, corresponds to the lifetime of C*-TPT residing near head groups of RM, whereas the short lifetime component may be attributed to the C*-TPT near the central "water pool" of RM. Strong electrostatic interaction between the negatively charged AOT head groups and the positively charged drug molecule may be responsible for the long lifetime of cationic species residing at the interface of RM. Decrease in average lifetime of C*-TPT suggests that the cationic species gradually move toward the central pool of RM, and thereby, cationic species start a photoprotolytic reaction. The location of the probe will be confirmed by the time-resolved anisotropy measurement discussed in the later part of the manuscript.

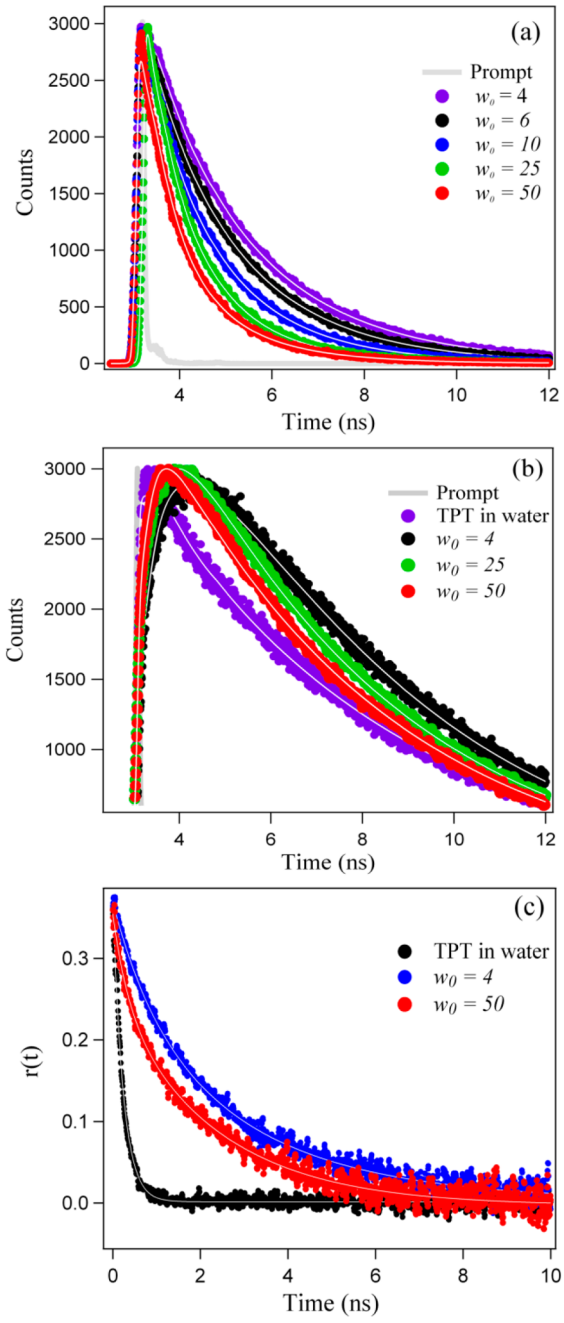

Figure 2. Fluorescence transients of TPT (excited at 375 nm) in reverse micelles with progressively increasing water content (w_0). (a) $\lambda_{collection}$ = 420 nm, (b) $\lambda_{collection}$ = 570 nm, and (c) fluorescence anisotropy transients of TPT ($\lambda_{collection}$ = 520 nm) in reverse micelles and in bulk water.

In order to avoid a minimal overlap from the emission of C*-TPT, the time-resolved fluorescence signals from Z*-TPT in water-RMs were collected at 570 nm (Figure 2b). Completely different and novel characteristic features come out when the time-resolved fluorescence signals from Z*-TPT in water-RMs were collected at 570 nm (Figure 2b). The decay profiles consist of two components (Table 1): one long nanosecond component (~5 ns) and another rise component (0.25−1 ns). The ~5 ns component is assigned to be the lifetime of Z*-TPT.[13−15] Surprisingly, the shorter component (0.25−1 ns) has a negative pre-exponential factor (Table 1). The negative amplitudes (or pre-exponential factor) indicate that there exists an excited-state process which generates a new emitting state that is different from the initially excited cationic species.[72] Notably, although we selectively excited (λ_{ex} = 375 nm) the cationic species, we are observing the emission from the zwitterionic species and it is attributed to the excited state proton transfer (ESPT) from the −OH group of TPT to the water molecule.[13,14] Thus, the negative pre-exponential factor appeared in the decay profile provides the direct support for the conversion from C* to Z*. The increment in the percentage of long lifetime component (~5.0 ns) with the increase in water content of the RM suggests that the population of Z* species hikes inside the RM. The slightly increased lifetime of Z*-TPT (Table 1) indicates that Z*-TPT is gaining stability inside the RM. It is well-known that the extent of proton activity increases as water content inside the RM increases;[30,49,50,56] hence, it facilitates the conversion of cationic (C*) form to zwitterions (Z*) via ESPT process. Generally, the rise time appearing in the decay profile indicates the existence of excited state dynamics, which is coming from the previously excited state. Therefore, the growth component appeared in the decay profile indicates the dynamics of ESPT process by which C* is converted to Z* species. Notably, the decay profile of TPT in bulk water is devoid of any growth component (Figure 2b), indicating that the ESPT dynamics are too fast to be detected by our TCSPC setup. Here it is relevant to mention that Douhal group reported slow proton transfer dynamics even in bulk water, although the contribution is much less (5%). The different observations by us and Douhal groups may be

dx.doi.org/10.1021/jp5066902 | J. Phys. Chem. B 2015, 119, 2363−2371

Table 1. Fluorescence Decay Parameters of TPT in Water Reverse Micelles (λ_{ex} = 375 nm)

w_0	$\lambda_{collection}$	τ_1 (ns)	τ_2 (ns)	τ_3 (ns)	R_1	R_2	R_3	τ_{avg} [a] (ns)	χ^2
water	570 nm	0.63	–	5.93	0.13	–	0.87	5.24	1.01
w_0 = 0	570 nm	1.24	–	4.47	0.26	–	0.74	3.63	1.02
w_0 = 4	420 nm	0.85	2.51	–	0.19	0.81	–	2.19	0.86
	570 nm	1.01	–	5.07	−0.35	–	0.65	3.64	1.15
w_0 = 10	420 nm	0.69	1.94	–	0.34	0.66	–	1.52	1.02
	570 nm	0.63	–	5.03	−0.35	–	0.65	3.51	1.08
w_0 = 15	420 nm	0.57	1.60	–	0.46	0.54	–	1.12	1.04
	570 nm	0.49	–	5.19	−0.32	–	0.68	3.66	1.04
w_0 = 25	420 nm	0.51	1.47	–	0.52	0.48	–	0.97	1.12
	570 nm	0.42	–	5.26	−0.31	–	0.69	3.77	1.04
w_0 = 50	420 nm	0.50	1.42	–	0.57	0.43	–	0.89	1.19
	570 nm	0.30	–	5.28	−0.30	–	0.70	3.76	1.06
w_0 = 70	420 nm	0.42	1.30	–	0.58	0.42	–	0.79	1.25
	570 nm	0.25	–	5.27	−0.30	–	0.70	3.76	1.07

[a] $\tau_{avg} = R_1\tau_1 + R_2\tau_2 + R_3\tau_3$.

attributed to the different instrument response of the TCSPC setup. A closer look at time-resolved results indicate that the lifetime of the growth component reduces (Table 1), inferring that the rate of ESPT dynamics becomes faster as the water content of the RM increases. Notably, the dynamics of proton transfer is dramatically affected by the ability of the solvent to reorganize.[56,73] The observed dynamics also depends on the proton mobility, that is, the ability of the hydronium ion to move away from the resulting anion. These properties make excited-state proton transfer (ESPT) a suitable probe for monitoring the local water environment. It was reported that, for small water pool of RMs, the orientational relaxation of water is much slower than in bulk water and becomes increasingly fast as the size of RM increases.[31,32,37,40,74] The slow rates of water orientational relaxation in nanoscopic water environments demonstrate that the timescale for hydrogen bond network rearrangement is slowed down substantially. As a consequence, ESPT dynamics, which depends on the dynamics of the H-bonded network, becomes sluggish at lower water content of the RMs, and it gradually accelerates as the behavior of water approaches the bulk. The presence of positively charged counterions (Na^+ ions) inside the RM may also have a significant role on the observed slow ESPT dynamics. In the absence of any ions in bulk water, the proton transfer takes place directly to the water molecule without any intervention, as water molecules are not involved in electrostatic/hydrogen bond interactions with the counterions. Thus, we believe that the ESPT dynamics inside RM is slowed down possibly also due to the screening effect of the sodium ions presented at the interface of the RM. In fact, there are reports where it has been observed that ESPT dynamics of HPTS get affected by the presence of salt.[75] The variation of polarity inside RM with respect to water content may also play a crucial role in slowing down the proton transfer dynamics, as it is known that PT dynamics of TPT is also dependent on the polarity of the surrounding environments.[13−16] In order to further elucidate this ESPT process, we have performed a kinetic isotope effect (KIE) experiment and found a considerable (1.7 times) KIE effect when H_2O is replaced by D_2O inside RM (Table S2, Note S1 of the Supporting Information).

To get insight into the geminate recombination process, which is opposite of the reversible or irreversible recombination of proton to the zwitterionic form of the drug, we have analyzed the time-resolved data around 520 nm (Table S1 of the Supporting Information) for verifying the presence of any extra component, which we might have missed in the decay profiles collected at the red-end side of the emission spectra. Here, the time-resolved data consists of three components, among which two components are very much similar to that of those obtained in the decay profiles monitored at 570 nm. The third ∼3 ns component is coming out from the cationic species of the drug,[15] as the emission of cationic species also contributes toward the 520 nm peak. Thus, we confirm the that geminate recombination process is not present in our system possibly because of the presence of sodium ions in the nearby vicinity of the drug, which can prevent diffusion of the proton toward the zwitterionic form of the drug. The other possibility is that geminate recombination is too fast to be detected by our setup.

To confirm the presence of two different types of species in the excited state, we have constructed a time-resolved area normalized emission spectrum (TRANES), a recently developed technique to explore excited state components. TRANES method is a one-step extension of the commonly used time-resolved emission spectrum (TRES) analysis.[76,77] TRANES and TRES of TPT inside the water-RM are depicted in Figure 3 and Figure S1 of the Supporting Information, respectively. It is clear from the figure that the emission intensity of C*-TPT progressively decreases with time, whereas the intensity of Z*-TPT gradually rises up. This observation reinforces our claim that the Z* form of the drug is generated at the cost of the C* form. The timescales at which the Z* form appeared are ∼1.02 ns and ∼700 and 280 ps for w_0 = 4, 10, and 50, respectively. These timescales are in good agreement with the respective growth component obtained in the decay profiles collected at 570 nm (Table 1). Moreover, a clear iso-emissive point at ∼480 nm in all above-mentioned w_0 values suggests that two different types of emissive species (C* and Z* forms) are present in the excited state.

3.3. Time-Resolved Fluorescence Anisotropy Measurements. It is well-established that time-resolved anisotropy measurements can provide important information about the rotational motion of fluorophore, which directly reflects the extent of restriction imposed by the surrounding environment.[78] Thus, time-resolved anisotropy measurements have been employed to probe the encapsulation process of TPT inside the RMs. The information regarding the rotational relaxation of TPT in bulk water and water containing RMs are

dx.doi.org/10.1021/jp5066902 | J. Phys. Chem. B 2015, 119, 2363−2371

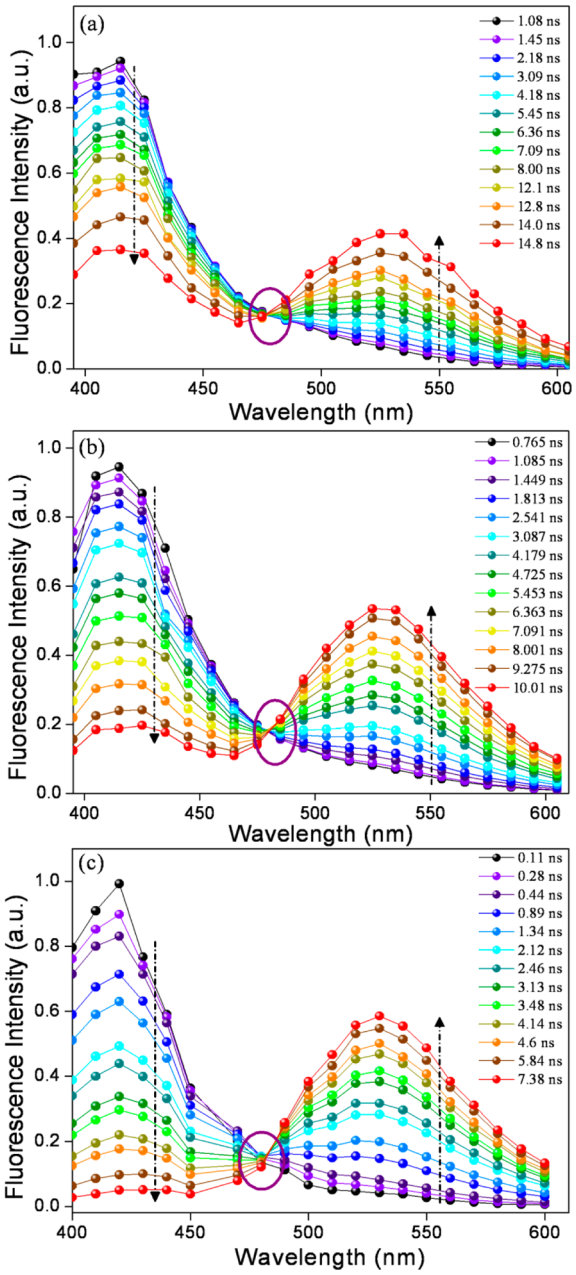

Figure 3. Time-resolved area normalized emission spectra (TRANES) of TPT in reverse micelle (λ_{ex} = 375 nm) at (a) w_0 = 4, (b) w_0 = 10, and (c) w_0 = 50.

gathered by probing the time-resolved fluorescence anisotropy of the zwitterionic form of TPT at 525 nm. The decay profiles are shown in Figure 2c and corresponding results are summarized in Table 2. The rotational relaxation time (τ_r) of drug molecule in bulk water is 216 ps and single exponential in nature. However, the decays are biexponential in nature in RMs. The biexponential decay is fitted by the equation

$$r(t) = r_0\left[f_1 \exp\left(\frac{-t}{\tau_{1r}}\right) + f_2 \exp\left(\frac{-t}{\tau_{2r}}\right)\right]$$

where r_0 is the limiting anisotropy to represent the inherent depolarization of the probe molecule, τ_{1r} and τ_{2r} are the fast and slow rotational relaxation components of the probe molecule inside RM, respectively, and f_1 and f_2 are the relative amplitudes of two components, respectively. To get an overall idea, the average rotational relaxation time has been calculated and it becomes 2.4, 2.1 and 1.8 ns for w_0 = 4, 25, and 50, respectively. The significant increment in rotational relaxation time in RMs compared to water infers that the drug molecules reside in highly restricted milieu. The faster rotational motion of TPT with an increasing w_0 value indicates that drug molecules are experiencing slightly less restricted environments, as the size of the RM increases. For detailed understanding of the biexponential behavior of anisotropy decays, we have used the wobbling-in-a-cone model[33,51,79] (Note S2 of the Supporting Information). In this model, the order parameter (S^2) can be used for understanding the location of the probe inside the RM. The order parameter describes the equilibrium orientational distribution of the probe inside the RM. S = 0 indicates that the motion is completely free, whereas S = 1 corresponds to the completely restricted environment. Here in our systems, the estimated S value varies from 0.831 at w_0 = 4 to 0.837 at w_0 = 50 (Table 2). Moreover, the cone angle $\theta°$ calculated (Table 2) from the order parameter varies from 28.05° (at w_0 = 4) and 27.52° (at w_0 = 50) and the values are in accordance with the previous findings.[33,79] As the order parameters and cone angles did not change significantly with the w_0 values, we believe that TPT is not located at the central "water pool" but closer to the interface (even at higher water content of the RM) and still feels the effect of both bound water and sodium counterions.

Even though few organic probes (HPTS,[49,50,56] D-luciferin,[62] 7HQ,[58−60] 2N68DS,[29] 2PBI,[57] 7H4MC,[73] and MFOH,[65] etc.) are used to understand the role of water inside RMs by excited state intermolecular proton transfer (ESPT) process, ESPT dynamics of a potential anticancer drug, TPT, is being probed for the first time inside the nanocavity of RM. The significant essence of the present work is that we could be able to directly monitor the ESPT process of TPT from the conversion dynamics of the excited state cationic (C*) to the zwitterionic (Z*) forms of the drug. Notably, the ESPT dynamics of TPT is ultrafast in bulk water; however, the ESPT dynamics is slowed down drastically when TPT is entrapped inside the RM. The sluggish ESPT dynamics of TPT is an outcome of several impacts. The combined effects of nanoconfinement and slow

Table 2. Time-Resolved Fluorescence Anisotropy Fitting Parameters of TPT in Reverse Micelles (λ_{ex} = 375 nm, $\lambda_{collection}$ = 520 nm)

sample	τ_{1r} (ns)	τ_{2r} (ns)	f_1	f_2	r_0	S	$\theta°$	$\langle\tau_r\rangle^a$ (ns)	χ^2
water	–	0.22	–	1.00	0.39	–	–	0.22	1.16
w_0 = 4	0.91	3.05	0.31	0.69	0.38	0.83	28.05	2.40	1.02
w_0 = 25	0.38	2.80	0.29	0.71	0.36	0.84	26.98	2.09	1.06
w_0 = 50	0.36	2.42	0.30	0.70	0.37	0.84	27.52	1.79	1.00

$^a\langle\tau_r\rangle = f_1\tau_{1r} + f_2\tau_{2r}$.

dx.doi.org/10.1021/jp5066902 | J. Phys. Chem. B 2015, 119, 2363−2371

solvation dynamics of water are believed to be responsible for the observed slow ESPT dynamics inside RM. The screening effects of counterions present at the interface of RM also have some role toward the ESPT dynamics. We believe that the present findings are important to elucidate the role of water in many biological functions and to understand small and fast structural changes in the water network, which are essential factors in proton transfer reactions. Moreover, the study of photophysical properties inside the RMs and its switchover from the C* form to the Z* form might be helpful in understanding the proton transfer dynamics of TPT inside a biological membrane and its function as photosensitizer trigger anticancer activity inside the tumor cell.

4. CONCLUSION

The photophysical properties of TPT have been studied in aqueous AOT reverse micelle (RM) by steady-state and time-resolved fluorescence measurements. In bulk water, TPT exhibits single emission, which is believed to be originated from a zwitterionic (Z*) form of the drug, as an outcome of the excited state proton transfer (ESPT) process from the excited state cationic (C*) form of TPT to the nearby water molecule. In AOT/*n*-heptane RM, the drug shows dual emission attributed to the simultaneous existence of both C* and Z* forms of the drug. The presence of single iso-emissive point in the time-resolved area normalized emission spectrum (TRANES) further confirms the coexistence of two species (C* and Z*) in the excited state. Interestingly, ESPT dynamics were found to be severely retarded within the polar nanocavity of RM, exhibiting a time constant of ∼250 ps to ∼1 ns, which is slower than the dynamics obtained for TPT in bulk water (30 ps). The retardation of EPST dynamics in RM compared to bulk water might be due to cumulative effects of nanoconfinement, disrupted hydrogen-bonding network of water molecules, and the screening of the sodium ions present at the interface.

■ ASSOCIATED CONTENT

Supporting Information

Table of fluorescence decay fitting parameters of TPT in water-RM collected at 520 nm; time-resolved emission spectra (TRES) of TPT in water-RM at various w_0 values; table of fluorescence decay parameters of TPT in D_2O-RM; measurement of kinetic isotope effect (KIE); and description of wobbling-in-a-cone model. This material is available free of charge via the Internet at http://pubs.acs.org.

■ AUTHOR INFORMATION

Corresponding Author

* E-mail: p.hazra@iiserpune.ac.in. Tel: +91-20-2590-8077. Fax: +91-20-2589 9790.

Notes

The authors declare no competing financial interest.

■ ACKNOWLEDGMENTS

P.H. is thankful to the Council of Scientific and Industrial Research (CSIR, Scheme no. 37(1499)/11/EMR-II) for financial support. R.K.K. is thankful to University Grant Commission (UGC) for providing Senior Research Fellowship (SRF), and A.S. is thankful to CSIR for providing the CSIR-SRF fellowship. Authors thank IISER-Pune for providing excellent experimental facilities. Authors are thankful to anonymous referees for their valuable comments and suggestions.

■ REFERENCES

(1) Wall, M. E.; Wani, M. C.; Cook, C. E.; Palmer, K. H.; McPhail, A. T.; Sim, G. A. Plant Antitumor Agents. I. The Isolation and Structure of Camptothecin, a Novel Alkaloidal Leukemia and Tumor Inhibitor from Camptotheca acuminata1,2. *J. Am. Chem. Soc.* **1966**, *88*, 3888−3890.

(2) Pommier, Y. Topoisomerase I Inhibitors: Camptothecins and Beyond. *Nat. Rev. Cancer* **2006**, *6*, 789−802.

(3) Garcia-Carbonero, R.; Supko, J. G. Current Perspectives on the Clinical Experience, Pharmacology, and Continued Development of the Camptothecins. *Clin. Cancer Res.* **2002**, *8*, 641−661.

(4) Hartwell, D.; Jones, J.; Loveman, E.; Harris, P.; Clegg, A.; Bird, A. Topotecan for Relapsed Small Cell Lung Cancer: A Systematic Review and Economic Evaluation. *Cancer Treat. Rev.* **2011**, *37*, 242−249.

(5) Siu, F.-M.; Che, C.-M. Persistence of Camptothecin Analog−Topoisomerase I−DNA Ternary Complexes: A Molecular Dynamics Study. *J. Am. Chem. Soc.* **2008**, *130*, 17928−17937.

(6) Kollmannsberger, C.; Mross, K.; Jakob, A.; Kanz, L.; Bokemeyer, C. Topotecan: A Novel Topoisomerase I Inhibitor: Pharmacology and Clinical Experience. *Oncology* **1999**, *56*, 1−12.

(7) Kurtz, J. E.; Freyer, G.; Joly, F.; Gladieff, L.; Kaminski, M. C.; Fabbro, M.; Floquet, A.; Hardy-Bessard, A. C.; Raban, N.; Ray-Coquard, I.; Pujade-Lauraine, E. On Behalf Of The Gineco Group, F. Combined Oral Topotecan plus Carboplatin in Relapsed or Advanced Cervical Cancer: A GINECO Phase I-II Trial. *Anticancer Res.* **2012**, *32*, 1045−1049.

(8) Mirchandani, D.; Hochster, H.; Hamilton, A.; Liebes, L.; Yee, H.; Curtin, J. P.; Lee, S.; Sorich, J.; Dellenbaugh, C.; Muggia, F. M. Phase I Study of Combined Pegylated Liposomal Doxorubicin with Protracted Daily Topotecan for Ovarian Cancer. *Clin. Cancer Res.* **2005**, *11*, 5912−5919.

(9) Lalloo, A.; Chao, P.; Hu, P.; Stein, S.; Sinko, P. J. Pharmacokinetic and Pharmacodynamic Evaluation of a Novel in Situ Forming Poly(Ethylene Glycol)-Based Hydrogel for the Controlled Delivery of the Camptothecins. *J. Controlled Release* **2006**, *112*, 333−342.

(10) Leppard, J.; Champoux, J. Human DNA Topoisomerase I: Relaxation, Roles, and Damage Control. *Chromosoma* **2005**, *114*, 75−85.

(11) Burke, T. G.; Malak, H.; Gryczynski, I.; Mi, Z.; Lakowicz, J. R. Fluorescence Detection of the Anticancer Drug Topotecan in Plasma and Whole Blood by Two-Photon Excitation. *Anal. Biochem.* **1996**, *242*, 266−270.

(12) Vogt, F. G.; Dell'Orco, P. C.; Diederich, A. M.; Su, Q.; Wood, J. L.; Zuber, G. E.; Katrincic, L. M.; Mueller, R. L.; Busby, D. J.; DeBrosse, C. W. A Study of Variable Hydration States in Topotecan Hydrochloride. *J. Pharm. Biomed. Anal.* **2006**, *40*, 1080−1088.

(13) di Nunzio, M. R.; Wang, Y.; Douhal, A. Structural Photodynamic Behavior of Topotecan, a Potent Anticancer Drug, in Aqueous Solutions at Different pHs. *J. Phys. Chem. B* **2012**, *116*, 8182−8190.

(14) di Nunzio, M. R.; Wang, Y.; Douhal, A. Structural Spectroscopy and Dynamics of Inter- and Intramolecular H-Bonding Interactions of Topotecan, a Potent Anticancer Drug, in Organic Solvents and in Aqueous Solution. *J. Phys. Chem. B* **2012**, *116*, 7522−7530.

(15) Gavvala, K.; Sengupta, A.; Koninti, R. K.; Hazra, P. Supramolecular Host-Inhibited Excited-State Proton Transfer and Fluorescence Switching of the Anti-Cancer Drug, Topotecan. *ChemPhysChem* **2013**, *14*, 3375−3383.

(16) di Nunzio, M. R.; Wang, Y.; Douhal, A. Spectroscopy and Dynamics of Topotecan Anti-Cancer Drug Comprised within Cyclodextrins. *J. Photochem. Photobiol., A* **2013**, *266*, 12−21.

(17) Tardi, P.; Choice, E.; Masin, D.; Redelmeier, T.; Bally, M.; Madden, T. D. Liposomal Encapsulation of Topotecan Enhances Anticancer Efficacy in Murine and Human Xenograft Models. *Cancer Res.* **2000**, *60*, 3389−3393.

(18) Foulon, C.; Tedou, J.; Queruau Lamerie, T.; Vaccher, C.; Bonte, J. P.; Goossens, J. F. Assessment of the Complexation Degree of Camptothecin Derivatives and Cyclodextrins Using Spectroscopic and Separative Methodologies. *Tetrahedron: Asymmetry* **2009**, *20*, 2482−2489.
(19) Wang, G.-S.; Zhang, H.-Y.; Ding, F.; Liu, Y. Preparation and Characterization of Inclusion Complexes of Topotecan with Sulfonatocalixarene. *J. Inclusion Phenom. Macrocyclic Chem.* **2011**, *69*, 85−89.
(20) Luisi, P. L.; Straub, B. E. *Reverse Micelles: Bilogical and Technological Relevance of Amphiphilic Structure in Apolar Media*, 1st ed.; Springer: New York, 1999.
(21) Kalyanasundaram, K. Photoprocesses in Reversed Micelles and in Microemulsions. In *Photochemistry in Microheterogeneous Systems*, Kalyanasundaram, K., Ed.; Academic Press: Waltham, MA, 1987; Chapter 5, pp 143−172.
(22) Nandi, N.; Bhattacharyya, K.; Bagchi, B. Dielectric Relaxation and Solvation Dynamics of Water in Complex Chemical and Biological Systems. *Chem. Rev.* **2000**, *100*, 2013−2046.
(23) Bhattacharyya, K. Solvation Dynamics and Proton Transfer in Supramolecular Assemblies. *Acc. Chem. Res.* **2002**, *36*, 95−101.
(24) Crans, D. C.; Levinger, N. E. The Conundrum of pH in Water Nanodroplets: Sensing pH in Reverse Micelle Water Pools. *Acc. Chem. Res.* **2012**, *45*, 1637−1645.
(25) Levinger, N. E.; Swafford, L. A. Ultrafast Dynamics in Reverse Micelles. *Annu. Rev. Phys. Chem.* **2009**, *60*, 385−406.
(26) Moyano, F.; Setien, E.; Silber, J. J.; Correa, N. M. Enzymatic Hydrolysis of *N*-Benzoyl-L-Tyrosine *p*-Nitroanilide by α-Chymotrypsin in DMSO-Water/AOT/*n*-Heptane Reverse Micelles. A Unique Interfacial Effect on the Enzymatic Activity. *Langmuir* **2013**, *29*, 8245−8254.
(27) Lee, L.-C.; Zhao, Y. Metalloenzyme-Mimicking Supramolecular Catalyst for Highly Active and Selective Intramolecular Alkyne Carboxylation. *J. Am. Chem. Soc.* **2014**, *136*, 5579−5582.
(28) Correa, N. M.; Silber, J. J.; Riter, R. E.; Levinger, N. E. Nonaqueous Polar Solvents in Reverse Micelle Systems. *Chem. Rev.* **2012**, *112*, 4569−4602.
(29) Cohen, B.; Huppert, D.; Solntsev, K. M.; Tsfadia, Y.; Nachliel, E.; Gutman, M. Excited State Proton Transfer in Reverse Micelles. *J. Am. Chem. Soc.* **2002**, *124*, 7539−7547.
(30) Piletic, I. R.; Moilanen, D. E.; Spry, D. B.; Levinger, N. E.; Fayer, M. D. Testing the Core/Shell Model of Nanoconfined Water in Reverse Micelles Using Linear and Nonlinear IR Spectroscopy. *J. Phys. Chem. A* **2006**, *110*, 4985−4999.
(31) Fayer, M. D. Dynamics of Water Interacting with Interfaces, Molecules, and Ions. *Acc. Chem. Res.* **2011**, *45*, 3−14.
(32) Levinger, N. E. Water in Confinement. *Science* **2002**, *298*, 1722−1723.
(33) Moilanen, D. E.; Fenn, E. E.; Wong, D.; Fayer, M. D. Water Dynamics at the Interface in AOT Reverse Micelles. *J. Phys. Chem. B* **2009**, *113*, 8560−8568.
(34) Martinez, A. V.; Dominguez, L.; Małolepsza, E.; Moser, A.; Ziegler, Z.; Straub, J. E. Probing the Structure and Dynamics of Confined Water in AOT Reverse Micelles. *J. Phys. Chem. B* **2013**, *117*, 7345−7351.
(35) Durantini, A. M.; Darío Falcone, R.; Silber, J. J.; Mariano Correa, N. More Evidence on the Control of Reverse Micelles Sizes. Combination of Different Techniques as a Powerful Tool to Monitor AOT Reversed Micelles Properties. *J. Phys. Chem. B* **2013**, *117*, 3818−3828.
(36) Pieniazek, P. A.; Lin, Y.-S.; Chowdhary, J.; Ladanyi, B. M.; Skinner, J. L. Vibrational Spectroscopy and Dynamics of Water Confined inside Reverse Micelles. *J. Phys. Chem. B* **2009**, *113*, 15017−15028.
(37) Baruah, B.; Roden, J. M.; Sedgwick, M.; Correa, N. M.; Crans, D. C.; Levinger, N. E. When Is Water Not Water? Exploring Water Confined in Large Reverse Micelles Using a Highly Charged Inorganic Molecular Probe. *J. Am. Chem. Soc.* **2006**, *128*, 12758−12765.
(38) Rosenfeld, D. E.; Schmuttenmaer, C. A. Dynamics of the Water Hydrogen Bond Network at Ionic, Nonionic, and Hydrophobic Interfaces in Nanopores and Reverse Micelles. *J. Phys. Chem. B* **2011**, *115*, 1021−1031.
(39) Orte, A.; Ruedas-Rama, M. J.; Paredes, J. M.; Crovetto, L.; Alvarez-Pez, J. M. Dynamics of Water-in-Oil Nanoemulsions Revealed by Fluorescence Lifetime Correlation Spectroscopy. *Langmuir* **2011**, *27*, 12792−12799.
(40) Biswas, R.; Furtado, J.; Bagchi, B. Layerwise Decomposition of Water Dynamics in Reverse Micelles: A Simulation Study of Two-Dimensional Infrared Spectrum. *J. Chem. Phys.* **2013**, *139*, 144906−144911.
(41) Jain, T. K.; Varshney, M.; Maitra, A. Structural Studies of Aerosol OT Reverse Micellar Aggregates by FT-IR Spectroscopy. *J. Phys. Chem.* **1989**, *93*, 7409−7416.
(42) Moilanen, D. E.; Levinger, N. E.; Spry, D. B.; Fayer, M. D. Confinement or the Nature of the Interface? Dynamics of Nanoscopic Water. *J. Am. Chem. Soc.* **2007**, *129*, 14311−14318.
(43) Harpham, M. R.; Ladanyi, B. M.; Levinger, N. E.; Herwig, K. W. Water Motion in Reverse Micelles Studied by Quasielastic Neutron Scattering and Molecular Dynamics Simulations. *J. Chem. Phys.* **2004**, *121*, 7855−7868.
(44) Quintana, S. S.; Falcone, R. D.; Silber, J. J.; Correa, N. M. Comparison between Two Anionic Reverse Micelle Interfaces: The Role of Water−Surfactant Interactions in Interfacial Properties. *ChemPhysChem* **2012**, *13*, 115−123.
(45) Falcone, R. D.; Silber, J. J.; Correa, N. M. What are the Factors that Control Non-Aqueous/AOT/n-Heptane Reverse Micelle Sizes? A Dynamic Light Scattering Study. *Phys. Chem. Chem. Phys.* **2009**, *11*, 11096−11100.
(46) Fenn, E. E.; Wong, D. B.; Giammanco, C. H.; Fayer, M. D. Dynamics of Water at the Interface in Reverse Micelles: Measurements of Spectral Diffusion with Two-Dimensional Infrared Vibrational Echoes. *J. Phys. Chem. B* **2011**, *115*, 11658−11670.
(47) Skinner, J. L.; Pieniazek, P. A.; Gruenbaum, S. M. Vibrational Spectroscopy of Water at Interfaces. *Acc. Chem. Res.* **2011**, *45*, 93−100.
(48) Thompson, W. H. Solvation Dynamics and Proton Transfer in Nanoconfined Liquids. *Annu. Rev. Phys. Chem.* **2011**, *62*, 599−619.
(49) Tielrooij, K. J.; Cox, M. J.; Bakker, H. J. Effect of Confinement on Proton-Transfer Reactions in Water Nanopools. *ChemPhysChem* **2009**, *10*, 245−251.
(50) Sedgwick, M.; Cole, R. L.; Rithner, C. D.; Crans, D. C.; Levinger, N. E. Correlating Proton Transfer Dynamics To Probe Location in Confined Environments. *J. Am. Chem. Soc.* **2012**, *134*, 11904−11907.
(51) Douhal, A.; Angulo, G.; Gil, M.; Organero, J. Á.; Sanz, M.; Tormo, L. Observation of Three Behaviors in Confined Liquid Water within a Nanopool Hosting Proton-Transfer Reactions. *J. Phys. Chem. B* **2007**, *111*, 5487−5493.
(52) Piletic, I. R.; Tan, H.-S.; Fayer, M. D. Dynamics of Nanoscopic Water: Vibrational Echo and Infrared Pump−Probe Studies of Reverse Micelles. *J. Phys. Chem. B* **2005**, *109*, 21273−21284.
(53) Tan, H.-S.; Piletic, I. R.; Riter, R. E.; Levinger, N. E.; Fayer, M. D. Dynamics of Water Confined on a Nanometer Length Scale in Reverse Micelles: Ultrafast Infrared Vibrational Echo Spectroscopy. *Phys. Rev. Lett.* **2005**, *94*, 057405.
(54) Rini, M.; Magnes, B.-Z.; Pines, E.; Nibbering, E. T. J. Real-Time Observation of Bimodal Proton Transfer in Acid-Base Pairs in Water. *Science* **2003**, *301*, 349−352.
(55) Mathias, G.; Marx, D. Structures and Spectral Signatures of Protonated Water Networks in Bacteriorhodopsin. *Proc. Natl. Acad. Sci. U.S.A.* **2007**, *104*, 6980−6985.
(56) Spry, D. B.; Goun, A.; Glusac, K.; Moilanen, D. E.; Fayer, M. D. Proton Transport and the Water Environment in Nafion Fuel Cell Membranes and AOT Reverse Micelles. *J. Am. Chem. Soc.* **2007**, *129*, 8122−8130.
(57) Mukherjee, T. K.; Panda, D.; Datta, A. Excited-State Proton Transfer of 2-(2′-Pyridyl)benzimidazole in Microemulsions: Selective

Enhancement and Slow Dynamics in Aerosol OT Reverse Micelles with an Aqueous Core. *J. Phys. Chem. B* **2005**, *109*, 18895−18901.
(58) Kwon, O.-H.; Kim, T. G.; Lee, Y.-S.; Jang, D.-J. Biphasic Tautomerization Dynamics of Excited 7-Hydroxyquinoline in Reverse Micelles. *J. Phys. Chem. B* **2006**, *110*, 11997−12004.
(59) Angulo, G.; Organero, J. A.; Carranza, M. A.; Douhal, A. Probing the Behavior of Confined Water by Proton-Transfer Reactions. *J. Phys. Chem. B* **2006**, *110*, 24231−24237.
(60) Park, S.-Y.; Kwon, O.-H.; Kim, T. G.; Jang, D.-J. Ground-State Proton Transfer of 7-Hydroxyquinoline Confined in Biologically Relevant Water Nanopools. *J. Phys. Chem. C* **2009**, *113*, 16110−16115.
(61) Sarangi, M. K.; Mitra, A. K.; Sengupta, C.; Ghosh, S.; Chakraborty, S.; Saha, C.; Basu, S. Hydrogen Bond Sensitive Probe 5-Methoxy-1-keto-1,2,3,4-tetrahydro Carbazole in the Microheterogeneity of Binary Mixtures and Reverse Micelles. *J. Phys. Chem. C* **2013**, *117*, 2166−2174.
(62) Kuchlyan, J.; Banik, D.; Kundu, N.; Ghosh, S.; Banerjee, C.; Sarkar, N. Effect of Confinement on Excited-State Proton Transfer of Firefly's Chromophore d-Luciferin in AOT Reverse Micelles. *J. Phys. Chem. B* **2014**, *118*, 3401−3408.
(63) Choudhury, S. D.; Pal, H. Modulation of Excited-State Proton-Transfer Reactions of 7-Hydroxy-4-methylcoumarin in Ionic and Nonionic Reverse Micelles. *J. Phys. Chem. B* **2009**, *113*, 6736−6744.
(64) Kwon, O.-H.; Jang, D.-J. Excited-State Double Proton Transfer of 7-Azaindole in Water Nanopools. *J. Phys. Chem. B* **2005**, *109*, 20479−20484.
(65) Mukhopadhyay, M.; Mandal, A.; Misra, R.; Banerjee, D.; Bhattacharyya, S. P.; Mukherjee, S. Nanopools Governing Proton Transfer in Diametrical Ways in the Ground and Excited State. *J. Phys. Chem. B* **2009**, *113*, 567−573.
(66) Gavvala, K.; Sengupta, A.; Hazra, P. Modulation of Photophysics and pKa Shift of the Anti-cancer Drug Camptothecin in the Nanocavities of Supramolecular Hosts. *ChemPhysChem* **2013**, *14*, 532−542.
(67) Gavvala, K.; Sasikala, W. D.; Sengupta, A.; Dalvi, S. A.; Mukherjee, A.; Hazra, P. Modulation of Excimer Formation of 9-(Dicyano-Vinyl)Julolidine by the Macrocyclic Hosts. *Phys. Chem. Chem. Phys.* **2013**, *15*, 330−340.
(68) Tan, H.-S.; Piletic, I. R.; Fayer, M. D. Orientational Dynamics of Water Confined on a Nanometer Length Scale in Reverse Micelles. *J. Chem. Phys.* **2005**, *122*, 174501−174509.
(69) Rafiq, S.; Yadav, R.; Sen, P. Microviscosity inside a Nanocavity: A Femtosecond Fluorescence Up-Conversion Study of Malachite Green. *J. Phys. Chem. B* **2010**, *114*, 13988−13994.
(70) Marques, B. S.; Nucci, N. V.; Dodevski, I.; Wang, K. W. C.; Athanasoula, E. A.; Jorge, C.; Wand, A. J. Measurement and Control of pH in the Aqueous Interior of Reverse Micelles. *J. Phys. Chem. B* **2014**, *118*, 2020−2031.
(71) Chowdhary, J.; Ladanyi, B. M. Molecular Dynamics Simulation of Aerosol-OT Reverse Micelles. *J. Phys. Chem. B* **2009**, *113*, 15029−15039.
(72) Novaira, M.; Biasutti, M. A.; Silber, J. J.; Correa, N. M. New Insights on the Photophysical Behavior of PRODAN in Anionic and Cationic Reverse Micelles: From Which State or States Does It Emit? *J. Phys. Chem. B* **2007**, *111*, 748−759.
(73) Choudhury, S. D.; Nath, S.; Pal, H. Excited-State Proton Transfer Behavior of 7-Hydroxy-4-methylcoumarin in AOT Reverse Micelles. *J. Phys. Chem. B* **2008**, *112*, 7748−7753.
(74) Patra, A.; Luong, T. Q.; Mitra, R. K.; Havenith, M. The Influence of Charge on the Structure and Dynamics of Water Encapsulated in Reverse Micelles. *Phys. Chem. Chem. Phys.* **2014**, *16*, 12875−12883.
(75) Leiderman, P.; Gepshtein, R.; Uritski, A.; Genosar, L.; Huppert, D. Effect of Electrolytes on the Excited-State Proton Transfer and Geminate Recombination. *J. Phys. Chem. A* **2006**, *110*, 5573−5584.
(76) Koti, A. S. R.; Periasamy, N. Application of Time Resolved Area Normalized Emission Spectroscopy to Multicomponent Systems. *J. Chem. Phys.* **2001**, *115*, 7094−7099.
(77) Koti, A. S. R.; Krishna, M. M. G.; Periasamy, N. Time-Resolved Area-Normalized Emission Spectroscopy (TRANES): A Novel Method for Confirming Emission from Two Excited States. *J. Phys. Chem. A* **2001**, *105*, 1767−1771.
(78) Lackowicz, J. R. *Principles of Fluorescence Spectroscopy*, 3rd ed.; Springer: New York, 2006.
(79) Chatterjee, A.; Maity, B.; Seth, D. The Photophysics of 7-(N,N[Prime or Minute]-Diethylamino)Coumarin-3-Carboxylic Acid in Water/AOT/Isooctane Reverse Micelles: an Excitation Wavelength Dependent Study. *Phys. Chem. Chem. Phys.* **2013**, *15*, 1894−1906.